Pion structure within a dynamical model in Minkowski space.

Wayne de Paula

Instituto Tecnológico de Aeronáutica - Brasil

Collaborators
E. Ydrefors (IMP/Lanzhou), D. Duarte (UFSM), JH. de Alvarenga Noronha,
T. Frederico (ITA) and G. Salmè (INFN/Roma)

Light Cone 2022 Online: Physics of Hadrons on the Light Front

Summary

Pion as a quark-antiquark bound state

Bound state: Solve the Bethe-Salpeter equation

Pion as a quark-antiquark bound state

Bound state: Solve the Bethe-Salpeter equation

Most non-perturbative methods are formulated in Euclidean space

Pion as a quark-antiquark bound state

Bound state: Solve the Bethe-Salpeter equation

Most non-perturbative methods are formulated in Euclidean space

Wick Rotation: We have to be care with the presence of singulatiries
Our challenge is to work with a non-perturbative framework in Minkowski Space in order to access hadron structure observables defined on the light-front.

Pion as a quark-antiquark bound state

Bound state: Solve the Bethe-Salpeter equation

Most non-perturbative methods are formulated in Euclidean space

Wick Rotation: We have to be care with the presence of singulatiries
Our challenge is to work with a non-perturbative framework in Minkowski Space in order to access hadron structure observables defined on the light-front.

Minkowski solutions: Bethe-Salpeter

Pion as a quark-antiquark bound state

Bound state: Solve the Bethe-Salpeter equation

Most non-perturbative methods are formulated in Euclidean space

Wick Rotation: We have to be care with the presence of singulatiries
Our challenge is to work with a non-perturbative framework in Minkowski Space in order to access hadron structure observables defined on the light-front.

Minkowski solutions: Bethe-Salpeter

Tool: Integral representation

Pion as a quark-antiquark bound state

Bethe-Salpeter equation (0^-) :

Pion as a quark-antiquark bound state

Bethe-Salpeter equation (0^-) :

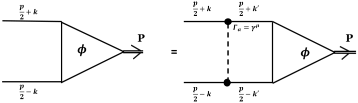

Pion as a quark-antiquark bound state

Bethe-Salpeter equation (0^-) :

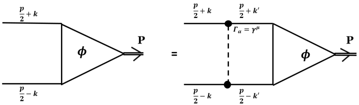

$$\begin{aligned} \Phi(k;P) &= S\left(k+\tfrac{P}{2}\right)\int \frac{d^4k'}{(2\pi)^4} S^{\mu\nu}(q)\Gamma_\mu(q)\Phi(k';P)\widehat{\Gamma}_\nu(q)S\left(k-\tfrac{P}{2}\right) \\ \widehat{\Gamma}_\nu(q) &= C\;\Gamma_\nu(q)\;C^{-1} \end{aligned}$$

where we use: i) bare propagators for the quarks and gluons;
ii) ladder approximation

$$S(P) = \frac{i}{\not{P}-m+i\epsilon}\,,\; S^{\mu\nu}(q) = -i\frac{g^{\mu\nu}}{q^2-\mu^2+i\epsilon}\,,\; \Gamma^\mu = ig\frac{\mu^2-\Lambda^2}{q^2-\Lambda^2+i\epsilon}\gamma^\mu\,,$$

Pion as a quark-antiquark bound state

Bethe-Salpeter equation (0^-) :

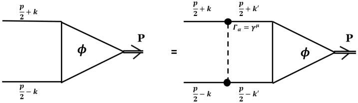

$$
\begin{aligned}
\Phi(k;P) &= S\left(k+\tfrac{P}{2}\right)\int \frac{d^4k'}{(2\pi)^4} S^{\mu\nu}(q)\Gamma_\mu(q)\Phi(k';P)\widehat{\Gamma}_\nu(q)S\left(k-\tfrac{P}{2}\right) \\
\widehat{\Gamma}_\nu(q) &= C\ \Gamma_\nu(q)\ C^{-1}
\end{aligned}
$$

where we use: i) bare propagators for the quarks and gluons;
ii) ladder approximation

$$
S(P) = \frac{i}{\not{P} - m + i\epsilon}\ ,\ S^{\mu\nu}(q) = -i\frac{g^{\mu\nu}}{q^2-\mu^2+i\epsilon}\ ,\ \Gamma^\mu = ig\frac{\mu^2-\Lambda^2}{q^2-\Lambda^2+i\epsilon}\gamma^\mu\ ,
$$

We consider only one of the Longitudinal components of the QGV

Pion as a quark-antiquark bound state

Bethe-Salpeter equation (0^-) :

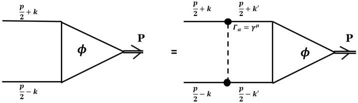

$$
\begin{aligned}
\Phi(k;P) &= S\left(k+\tfrac{P}{2}\right)\int \frac{d^4k'}{(2\pi)^4} S^{\mu\nu}(q)\Gamma_\mu(q)\Phi(k';P)\widehat{\Gamma}_\nu(q)S\left(k-\tfrac{P}{2}\right) \\
\widehat{\Gamma}_\nu(q) &= C\;\Gamma_\nu(q)\;C^{-1}
\end{aligned}
$$

where we use: i) bare propagators for the quarks and gluons;
ii) ladder approximation

$$
S(P) = \frac{i}{\not{P} - m + i\epsilon}\;,\; S^{\mu\nu}(q) = -i\frac{g^{\mu\nu}}{q^2-\mu^2+i\epsilon}\;,\; \Gamma^\mu = ig\frac{\mu^2-\Lambda^2}{q^2-\Lambda^2+i\epsilon}\gamma^\mu\;,
$$

We consider only one of the Longitudinal components of the QGV

We set the value of the scale parameter (300 MeV) from the combined analysis of Lattice simulations , the Quark-Gap Equation and Slanov-Taylor identity.

Oliveira, WP, Frederico, de Melo EPJC 78(7), 553 (2018) & EPJC 79 (2019) 116 & EPJC 80 (2020) 484

NIR for fermion-antifermion Bound State

BSA for a quark-antiquark bound state:

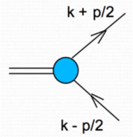

NIR for fermion-antifermion Bound State

BSA for a quark-antiquark bound state:

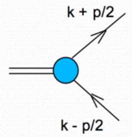

$$\Phi(k;P) = \sum_{i=1}^{4} S_i(k;P)\phi_i(k;P)$$

NIR for fermion-antifermion Bound State

BSA for a quark-antiquark bound state:

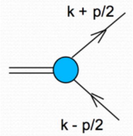

$$\Phi(k;P) = \sum_{i=1}^{4} S_i(k;P)\phi_i(k;P)$$

Dirac structures given by

NIR for fermion-antifermion Bound State

BSA for a quark-antiquark bound state:

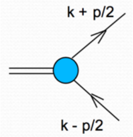

$$\Phi(k;P) = \sum_{i=1}^{4} S_i(k;P)\phi_i(k;P)$$

Dirac structures given by

$$S_1(k;P) = \gamma_5,\ S_2(k;P) = \frac{\not{P}}{M}\gamma_5,\ S_3(k;P) = \frac{k\cdot P}{M^3}\not{P}\gamma_5 - \frac{1}{M}\not{k}\gamma_5,\ S_4(k;P) = \frac{i}{M^2}\sigma^{\mu\nu}P_\mu k_\nu\gamma_5$$

NIR for fermion-antifermion Bound State

BSA for a quark-antiquark bound state:

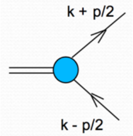

$$\Phi(k;P) = \sum_{i=1}^{4} S_i(k;P)\phi_i(k;P)$$

Dirac structures given by

$$S_1(k;P) = \gamma_5, \; S_2(k;P) = \frac{\not{P}}{M}\gamma_5, \; S_3(k;P) = \frac{k \cdot P}{M^3}\not{P}\gamma_5 - \frac{1}{M}\not{k}\gamma_5, \; S_4(k;P) = \frac{i}{M^2}\sigma^{\mu\nu}P_\mu k_\nu \gamma_5$$

Using the Nakanishi Integral Representation for the scalar functions

NIR for fermion-antifermion Bound State

BSA for a quark-antiquark bound state:

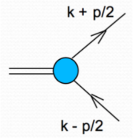

$$\Phi(k;P) = \sum_{i=1}^{4} S_i(k;P)\phi_i(k;P)$$

Dirac structures given by

$$S_1(k;P) = \gamma_5,\ \ S_2(k;P) = \frac{\not{P}}{M}\gamma_5,\ \ S_3(k;P) = \frac{k\cdot P}{M^3}\not{P}\gamma_5 - \frac{1}{M}\not{k}\gamma_5,\ \ S_4(k;P) = \frac{i}{M^2}\sigma^{\mu\nu}P_\mu k_\nu\gamma_5$$

Using the Nakanishi Integral Representation for the scalar functions

$$\phi_i(k;P) = \int_{-1}^{1} dz' \int_0^{\infty} d\gamma' \frac{g_i(\gamma', z'; \kappa^2)}{[k^2 + z'(P\cdot k) - \gamma' - \kappa^2 + i\epsilon]^3}$$

NIR for fermion-antifermion Bound State

BSA for a quark-antiquark bound state:

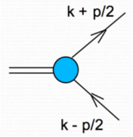

$$\Phi(k; P) = \sum_{i=1}^{4} S_i(k; P)\phi_i(k; P)$$

Dirac structures given by

$$S_1(k; P) = \gamma_5, \; S_2(k; P) = \frac{\not{P}}{M}\gamma_5, \; S_3(k; P) = \frac{k \cdot P}{M^3}\not{P}\gamma_5 - \frac{1}{M}\not{k}\gamma_5, \; S_4(k; P) = \frac{i}{M^2}\sigma^{\mu\nu}P_\mu k_\nu \gamma_5$$

Using the Nakanishi Integral Representation for the scalar functions

$$\phi_i(k; P) = \int_{-1}^{1} dz' \int_0^{\infty} d\gamma' \frac{g_i(\gamma', z'; \kappa^2)}{[k^2 + z'(P \cdot k) - \gamma' - \kappa^2 + i\epsilon]^3}$$

System of coupled integral equations

NIR for fermion-antifermion Bound State

BSA for a quark-antiquark bound state:

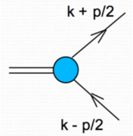

$$\Phi(k;P) = \sum_{i=1}^{4} S_i(k;P)\phi_i(k;P)$$

Dirac structures given by

$$S_1(k;P) = \gamma_5, \;\; S_2(k;P) = \frac{\not{P}}{M}\gamma_5, \;\; S_3(k;P) = \frac{k\cdot P}{M^3}\not{P}\gamma_5 - \frac{1}{M}\not{k}\gamma_5, \;\; S_4(k;P) = \frac{i}{M^2}\sigma^{\mu\nu}P_\mu k_\nu\gamma_5$$

Using the Nakanishi Integral Representation for the scalar functions

$$\phi_i(k;P) = \int_{-1}^{1} dz' \int_0^\infty d\gamma' \frac{g_i(\gamma', z'; \kappa^2)}{[k^2 + z'(P\cdot k) - \gamma' - \kappa^2 + i\epsilon]^3}$$

System of coupled integral equations

$$\int_{-1}^{1} dz' \int_0^\infty d\gamma' \frac{g_i(\gamma', z')}{[k^2 + z' p\cdot k - \gamma' - \kappa^2 + i\epsilon]^3} = \sum_j \int_{-1}^{1} dz' \int_0^\infty d\gamma' \; \mathcal{K}_{ij}(k,p;\gamma',z') \; g_j(\gamma',z')$$

Projecting BSE onto the LF hyper-plane $x^+ = 0$

Projecting BSE onto the LF hyper-plane $x^+ = 0$

Light-Front variables: $x^\mu = (x^+, x^-, \vec{x}_\perp)$

LF-time $x^+ = x^0 + x^3$
$$x^- = x^0 - x^3$$
$$\vec{x}_\perp = (x^1, x^2)$$

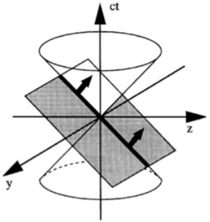

Projecting BSE onto the LF hyper-plane $x^+ = 0$

Light-Front variables: $x^\mu = (x^+, x^-, \vec{x}_\perp)$

LF-time $x^+ = x^0 + x^3$
$$x^- = x^0 - x^3$$
$$\vec{x}_\perp = (x^1, x^2)$$

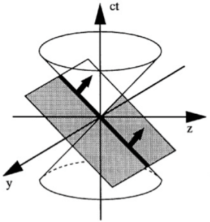

Within the LF framework, the valence wf is obtained by integrating the BSA on k- (elimination of the relative LF time).

Projecting BSE onto the LF hyper-plane $x^+ = 0$

Light-Front variables: $x^\mu = (x^+, x^-, \vec{x}_\perp)$

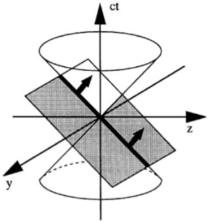

LF-time $x^+ = x^0 + x^3$

$$x^- = x^0 - x^3$$
$$\vec{x}_\perp = (x^1, x^2)$$

Within the LF framework, the valence wf is obtained by integrating the BSA on k- (elimination of the relative LF time).

LF amplitudes

Projecting BSE onto the LF hyper-plane $x^+ = 0$

Light-Front variables: $x^\mu = (x^+, x^-, \vec{x}_\perp)$

LF-time $x^+ = x^0 + x^3$
$x^- = x^0 - x^3$
$\vec{x}_\perp = (x^1, x^2)$

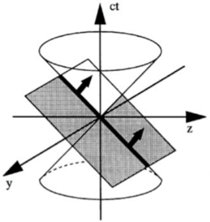

Within the LF framework, the valence wf is obtained by integrating the BSA on k- (elimination of the relative LF time).

LF amplitudes

$$\psi_i(\gamma,\xi) = \int \frac{dk^-}{2\pi}\ \phi_i(k,p) = -\frac{i}{M}\int_0^\infty d\gamma' \frac{g_i(\gamma', z; \kappa^2)}{[\gamma + \gamma' + m^2 z^2 + (1 - z^2)\kappa^2]^2}$$

Projecting BSE onto the LF hyper-plane $x^+ = 0$

Light-Front variables: $x^\mu = (x^+, x^-, \vec{x}_\perp)$

LF-time $x^+ = x^0 + x^3$
$x^- = x^0 - x^3$
$\vec{x}_\perp = (x^1, x^2)$

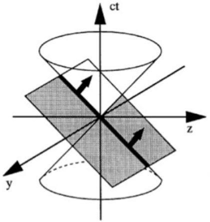

Within the LF framework, the valence wf is obtained by integrating the BSA on k- (elimination of the relative LF time).

LF amplitudes

$$\psi_i(\gamma, \xi) = \int \frac{dk^-}{2\pi}\ \phi_i(k, p) = -\frac{i}{M}\int_0^\infty d\gamma' \frac{g_i(\gamma', z; \kappa^2)}{[\gamma + \gamma' + m^2 z^2 + (1 - z^2)\kappa^2]^2}$$

The coupled equation system is (NIR+LF, Karmanov & Carbonell 2010)

Projecting BSE onto the LF hyper-plane $x^+ = 0$

Light-Front variables: $x^\mu = (x^+, x^-, \vec{x}_\perp)$

LF-time $x^+ = x^0 + x^3$

$$x^- = x^0 - x^3$$

$$\vec{x}_\perp = (x^1, x^2)$$

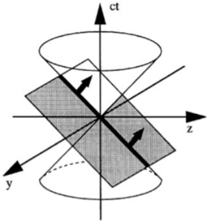

Within the LF framework, the valence wf is obtained by integrating the BSA on k- (elimination of the relative LF time).

LF amplitudes

$$\psi_i(\gamma, \xi) = \int \frac{dk^-}{2\pi}\ \phi_i(k, p) = -\frac{i}{M}\int_0^\infty d\gamma' \frac{g_i(\gamma', z; \kappa^2)}{\left[\gamma + \gamma' + m^2 z^2 + (1 - z^2)\kappa^2\right]^2}$$

The coupled equation system is (NIR+LF, Karmanov & Carbonell 2010)

$$\int_0^\infty \frac{d\gamma'\ g_i(\gamma', z; \kappa^2)}{\left[\gamma + \gamma' + m^2 z^2 + (1 - z^2)\kappa^2\right]^2} = iMg^2 \sum_j \int_0^\infty d\gamma' \int_{-1}^1 dz' \mathcal{L}_{ij}(\gamma, z; \gamma', z')\ g_j(\gamma', z'; \kappa^2)$$

The Kernel contains singular contributions

Parton distribution function

WP, Ydrefors, Nogueira, Frederico and Salmè PRD 105, L071505 (2022).

Parton distribution function

WP, Ydrefors, Nogueira, Frederico and Salmè PRD 105, L071505 (2022).

The unpolarized transverve-momentum distribution (uTMD) reads

$$f_1^q(\gamma,\xi) = \int d\phi_{\hat{\mathbf{k}}_\perp} \int \frac{dz^- d\mathbf{z}_\perp}{2(2\pi)^3} e^{i[\xi p^+ z^-/2 - \mathbf{k}_\perp \cdot \mathbf{z}_\perp]} \langle p|\bar{\psi}_q(-\frac{1}{2}z)\gamma^+\psi_q(\frac{1}{2}z)|p\rangle\Big|_{z^+=0}$$

Parton distribution function

WP, Ydrefors, Nogueira, Frederico and Salmè PRD 105, L071505 (2022).

The unpolarized transverve-momentum distribution (uTMD) reads

$$f_1^q(\gamma,\xi) = \int d\phi_{\hat{\mathbf{k}}_\perp} \int \frac{dz^- d\mathbf{z}_\perp}{2(2\pi)^3} e^{i[\xi p^+ z^-/2 - \mathbf{k}_\perp \cdot \mathbf{z}_\perp]} \langle p|\bar{\psi}_q(-\frac{1}{2}z)\gamma^+\psi_q(\frac{1}{2}z)|p\rangle\Big|_{z^+=0}$$

Considering the charge symmetry and Mandelstam framework

$$f_1(\gamma,\xi) = \frac{f_1^q(\gamma,\xi)+f_1^{\bar{q}}(\gamma,\xi)}{2} = \frac{1}{(2\pi)^4}\ \frac{1}{8}\int_{-\infty}^{\infty} dk^+ \delta(k^+ + P^+/2 - \xi P^+) \int_{-\infty}^{\infty} dk^- \int_0^{2\pi} d\phi_{\hat{\mathbf{k}}_\perp}$$
$$\times \left\{ Tr\Big[S^{-1}(k-P/2)\bar{\Phi}(k,P)\ \frac{\gamma^+}{2}\ \Phi(k,P)\Big] - Tr\Big[S^{-1}(k+P/2)\Phi(k,P)\ \frac{\gamma^+}{2}\ \bar{\Phi}(k,P)\Big] \right\}$$

Parton distribution function

WP, Ydrefors, Nogueira, Frederico and Salmè PRD 105, L071505 (2022).

The unpolarized transverve-momentum distribution (uTMD) reads

$$f_1^q(\gamma,\xi) = \int d\phi_{\hat{\mathbf{k}}_\perp} \int \frac{dz^- d\mathbf{z}_\perp}{2(2\pi)^3} e^{i[\xi p^+ z^-/2 - \mathbf{k}_\perp\cdot\mathbf{z}_\perp]} \langle p|\bar{\psi}_q(-\frac{1}{2}z)\gamma^+\psi_q(\frac{1}{2}z)|p\rangle\Big|_{z^+=0}$$

Considering the charge symmetry and Mandelstam framework

$$f_1(\gamma,\xi) = \frac{f_1^q(\gamma,\xi)+f_1^{\bar{q}}(\gamma,\xi)}{2} = \frac{1}{(2\pi)^4}\ \frac{1}{8}\int_{-\infty}^{\infty} dk^+\delta(k^+ + P^+/2 - \xi P^+)\int_{-\infty}^{\infty} dk^- \int_0^{2\pi} d\phi_{\hat{\mathbf{k}}_\perp}$$
$$\times\left\{Tr\Big[S^{-1}(k-P/2)\bar{\Phi}(k,P)\ \frac{\gamma^+}{2}\ \Phi(k,P)\Big] - Tr\Big[S^{-1}(k+P/2)\Phi(k,P)\ \frac{\gamma^+}{2}\ \bar{\Phi}(k,P)\Big]\right\}$$

The PDF is the integral over the squared transverse momentum

$$u(\xi) = \int_0^\infty d\gamma\ f_1(\gamma,\xi).$$

LF Momentum Distributions

LF Momentum Distributions

The fermionic field on the null-plane is given by:

$$\psi^{(+)}(\tilde{x}, x^+ = 0^+) = \int \frac{d\tilde{q}}{(2\pi)^{3/2}} \frac{\theta(q^+)}{\sqrt{2q^+}}$$

$$\sum_\sigma \left[U^{(+)}(\tilde{q},\sigma)\ b(\tilde{q},\sigma) e^{i\tilde{q}\cdot\tilde{x}} + V^{(+)}(\tilde{q},\sigma)\ d^\dagger(\tilde{q},\sigma) e^{-i\tilde{q}\cdot\tilde{x}} \right] ,$$

where

$$U^{(+)}(\tilde{q},\sigma) = \Lambda^+ u(\tilde{q},\sigma) \quad , \quad V^{(+)}(\tilde{q},\sigma) = \Lambda^+ v(\tilde{q},\sigma)$$

Hence, $d^\dagger$ and b are the fermion creation/annihilation operators

LF Momentum Distributions

The fermionic field on the null-plane is given by:

$$\psi^{(+)}(\tilde{x}, x^+ = 0^+) = \int \frac{d\tilde{q}}{(2\pi)^{3/2}} \, \frac{\theta(q^+)}{\sqrt{2q^+}}$$
$$\sum_\sigma \Big[U^{(+)}(\tilde{q},\sigma) \; b(\tilde{q},\sigma) e^{i\tilde{q}\cdot\tilde{x}} + V^{(+)}(\tilde{q},\sigma) \; d^\dagger(\tilde{q},\sigma) e^{-i\tilde{q}\cdot\tilde{x}} \Big] \; ,$$

where

$$U^{(+)}(\tilde{q},\sigma) = \Lambda^+ u(\tilde{q},\sigma) \quad , \quad V^{(+)}(\tilde{q},\sigma) = \Lambda^+ v(\tilde{q},\sigma)$$

Hence, $d^\dagger$ and b are the fermion creation/annihilation operators

The LF valence amplitude is the Fock component with the lowest number of constituents:

LF Momentum Distributions

The fermionic field on the null-plane is given by:

$$\psi^{(+)}(\tilde{x}, x^+ = 0^+) = \int \frac{d\tilde{q}}{(2\pi)^{3/2}} \frac{\theta(q^+)}{\sqrt{2q^+}}$$
$$\sum_\sigma \Big[U^{(+)}(\tilde{q},\sigma)\ b(\tilde{q},\sigma) e^{i\tilde{q}\cdot\tilde{x}} + V^{(+)}(\tilde{q},\sigma)\ d^\dagger(\tilde{q},\sigma) e^{-i\tilde{q}\cdot\tilde{x}} \Big] ,$$

where

$$U^{(+)}(\tilde{q},\sigma) = \Lambda^+ u(\tilde{q},\sigma) \quad , \quad V^{(+)}(\tilde{q},\sigma) = \Lambda^+ v(\tilde{q},\sigma)$$

Hence, $d^\dagger$ and b are the fermion creation/annihilation operators

The LF valence amplitude is the Fock component with the lowest number of constituents:

$$\varphi_2(\xi, \boldsymbol{k}_\perp, \sigma_i; M, J^\pi, J_z) = (2\pi)^3\ \sqrt{N_c}\ 2p^+ \sqrt{\xi(1-\xi)}\ \langle 0| b(\tilde{q}_2,\sigma_2)\ d(\tilde{q}_1,\sigma_1)|\tilde{p}, M, J^\pi, J_z\rangle\ ,$$

where $\tilde{q}_1 \equiv \{q_1^+ = M(1-\xi), -\mathbf{k}_\perp\}$, $\tilde{q}_2 \equiv \{q_2^+ = M\xi, \mathbf{k}_\perp\}$ and $\xi = 1/2 + k^+/p^+$.

LF Momentum Distributions

LF Momentum Distributions

LF valence amplitude in terms of BS amplitude is:

$$\varphi_2(\xi, \boldsymbol{k}_\perp, \sigma_i; M, J^\pi, J_z) = \frac{\sqrt{N_c}}{p^+} \frac{1}{4}\, \bar{u}_\alpha(\tilde{q}_2, \sigma_2) \int \frac{dk^-}{2\pi} \left[\gamma^+ \, \Phi(k,p)\, \gamma^+\right]_{\alpha\beta} v_\beta(\tilde{q}_1, \sigma_1) \;\; .$$

LF Momentum Distributions

LF valence amplitude in terms of BS amplitude is:

$$\varphi_2(\xi, \boldsymbol{k}_\perp, \sigma_i; M, J^\pi, J_z) \quad = \quad \frac{\sqrt{N_c}}{p^+}\frac{1}{4}\ \bar{u}_\alpha(\tilde{q}_2, \sigma_2)\int \frac{dk^-}{2\pi}\left[\gamma^+\ \Phi(k,p)\,\gamma^+\right]_{\alpha\beta}\ v_\beta(\tilde{q}_1, \sigma_1)\ \ .$$

which can be decomposed into two spin contributions:

LF Momentum Distributions

LF valence amplitude in terms of BS amplitude is:

$$\varphi_2(\xi, \boldsymbol{k}_\perp, \sigma_i; M, J^\pi, J_z) = \frac{\sqrt{N_c}}{p^+}\frac{1}{4}\,\bar{u}_\alpha(\tilde{q}_2, \sigma_2)\int \frac{dk^-}{2\pi}\left[\gamma^+\,\Phi(k,p)\,\gamma^+\right]_{\alpha\beta} v_\beta(\tilde{q}_1, \sigma_1) \;.$$

which can be decomposed into two spin contributions:

Anti-aligned configuration:

$$\psi_{\uparrow\downarrow}(\gamma, z) = \psi_2(\gamma, z) + \frac{z}{2}\psi_3(\gamma, \xi) + \frac{i}{M^3}\int_0^\infty d\gamma' \,\frac{\partial g_3(\gamma', z)/\partial z}{\gamma + \gamma' + z^2 m^2 + (1 - z^2)\kappa^2}$$

LF Momentum Distributions

LF valence amplitude in terms of BS amplitude is:

$$\varphi_2(\xi, \boldsymbol{k}_\perp, \sigma_i; M, J^\pi, J_z) \quad = \quad \frac{\sqrt{N_c}}{p^+} \frac{1}{4} \; \bar{u}_\alpha(\tilde{q}_2, \sigma_2) \int \frac{dk^-}{2\pi} \left[\gamma^+ \; \Phi(k,p)\, \gamma^+\right]_{\alpha\beta} \; v_\beta(\tilde{q}_1, \sigma_1) \quad .$$

which can be decomposed into two spin contributions:

Anti-aligned configuration:

$$\psi_{\uparrow\downarrow}(\gamma, z) = \psi_2(\gamma, z) + \frac{z}{2}\psi_3(\gamma, \xi) + \frac{i}{M^3} \int_0^\infty d\gamma' \; \frac{\partial g_3(\gamma', z)/\partial z}{\gamma + \gamma' + z^2 m^2 + (1 - z^2)\kappa^2}$$

Aligned configuration:

$$\psi_{\uparrow\uparrow}(\gamma, z) = \psi_{\downarrow\downarrow}(\gamma, z) = \frac{\sqrt{\gamma}}{M} \; \psi_4(\gamma, z)$$

LF Momentum Distributions

LF valence amplitude in terms of BS amplitude is:

$$\varphi_2(\xi, \boldsymbol{k}_\perp, \sigma_i; M, J^\pi, J_z) \quad = \quad \frac{\sqrt{N_c}}{p^+}\frac{1}{4}\ \bar{u}_\alpha(\tilde{q}_2, \sigma_2)\int\frac{dk^-}{2\pi}\left[\gamma^+\ \Phi(k,p)\,\gamma^+\right]_{\alpha\beta}\ v_\beta(\tilde{q}_1, \sigma_1)\ \ .$$

which can be decomposed into two spin contributions:

Anti-aligned configuration:

$$\psi_{\uparrow\downarrow}(\gamma, z) = \psi_2(\gamma, z) + \frac{z}{2}\psi_3(\gamma, \xi) + \frac{i}{M^3}\ \int_0^\infty d\gamma'\ \frac{\partial g_3(\gamma', z)/\partial z}{\gamma + \gamma' + z^2m^2 + (1-z^2)\kappa^2}$$

Aligned configuration:

$$\psi_{\uparrow\uparrow}(\gamma, z) = \psi_{\downarrow\downarrow}(\gamma, z) = \frac{\sqrt{\gamma}}{M}\ \psi_4(\gamma, z)$$

with the LF amplitudes given by

$$\psi_i(\gamma, z) = -\frac{i}{M}\int_0^\infty d\gamma'\frac{g_i(\gamma', z)}{[\gamma + \gamma' + m^2z^2 + (1-z^2)\kappa^2]^2}$$

Valence probability

Valence probability

The Fock expansion allows to restore a probabilistic framework.

The Valence Probability is:

$$P_{val} = \frac{1}{(2\pi)^3} \sum_{\sigma_1\sigma_2} \int_{-1}^{1} \frac{dz}{(1-z^2)} \int d\mathbf{k}_\perp \Big| \varphi_{n=2}(\xi, \boldsymbol{k}_\perp, \sigma_i; M, J^\pi, J_z) \Big|^2$$

Valence probability

The Fock expansion allows to restore a probabilistic framework.

The Valence Probability is:

$$P_{val} = \frac{1}{(2\pi)^3} \sum_{\sigma_1\sigma_2} \int_{-1}^{1} \frac{dz}{(1-z^2)} \int d\mathbf{k}_\perp \left| \varphi_{n=2}(\xi, \boldsymbol{k}_\perp, \sigma_i; M, J^\pi, J_z) \right|^2$$

In terms of the aligned and anti-aligned LFWF, we have

$$P_{val} = \int_{-1}^{1} dz \int_0^\infty \frac{d\gamma}{(4\pi)^2} \left[|\psi_{\uparrow\downarrow}(\gamma, z)|^2 + |\psi_{\uparrow\uparrow}(\gamma, z)|^2 \right],$$

Valence probability

The Fock expansion allows to restore a probabilistic framework.

The Valence Probability is:

$$P_{val} = \frac{1}{(2\pi)^3} \sum_{\sigma_1\sigma_2} \int_{-1}^{1} \frac{dz}{(1-z^2)} \int d\mathbf{k}_\perp \left| \varphi_{n=2}(\xi, \boldsymbol{k}_\perp, \sigma_i; M, J^\pi, J_z) \right|^2$$

In terms of the aligned and anti-aligned LFWF, we have

$$P_{val} = \int_{-1}^{1} dz \int_0^\infty \frac{d\gamma}{(4\pi)^2} \left[|\psi_{\uparrow\downarrow}(\gamma, z)|^2 + |\psi_{\uparrow\uparrow}(\gamma, z)|^2 \right],$$

The contribution to the PDF from the LF-valence WF is

$$u_{val}(\xi) = \int_0^\infty \frac{d\gamma}{(4\pi)^2} \left[|\psi_{\uparrow\downarrow}(\gamma, z)|^2 + |\psi_{\uparrow\uparrow}(\gamma, z)|^2 \right]$$

Quantitative results: Static properties

WP, Ydrefors, Nogueira, Frederico and Salme PRD 103 014002 (2021).

Quantitative results: Static properties

WP, Ydrefors, Nogueira, Frederico and Salme PRD 103 014002 (2021).

Set	m (MeV)	B/m	μ/m	Λ/m	P_{val}	$P_{\uparrow\downarrow}$	$P_{\uparrow\uparrow}$	f_π (MeV)
I	187	1.25	0.15	2	0.64	0.55	0.09	77
II	255	1.45	1.5	1	0.65	0.55	0.10	112
III	255	1.45	2	1	0.66	0.56	0.11	117
IV	215	1.35	2	1	0.67	0.57	0.11	98
V	187	1.25	2	1	0.67	0.56	0.11	84
VI	255	1.45	2.5	1	0.68	0.56	0.11	122
VII	255	1.45	2.5	1.1	0.69	0.56	0.12	127
VIII	255	1.45	2.5	1.2	0.70	0.57	0.13	130
IX	255	1.45	1	2	0.70	0.57	0.14	134
X	215	1.35	1	2	0.71	0.57	0.14	112
XI	187	1.25	1	2	0.71	0.58	0.14	96

Quantitative results: Static properties

WP, Ydrefors, Nogueira, Frederico and Salme PRD 103 014002 (2021).

Set	m (MeV)	B/m	μ/m	Λ/m	P_{val}	$P_{\uparrow\downarrow}$	$P_{\uparrow\uparrow}$	f_π (MeV)
I	187	1.25	0.15	2	0.64	0.55	0.09	77
II	255	1.45	1.5	1	0.65	0.55	0.10	112
III	255	1.45	2	1	0.66	0.56	0.11	117
IV	215	1.35	2	1	0.67	0.57	0.11	98
V	187	1.25	2	1	0.67	0.56	0.11	84
VI	255	1.45	2.5	1	0.68	0.56	0.11	122
VII	255	1.45	2.5	1.1	0.69	0.56	0.12	127
VIII	255	1.45	2.5	1.2	0.70	0.57	0.13	130
IX	255	1.45	1	2	0.70	0.57	0.14	134
X	215	1.35	1	2	0.71	0.57	0.14	112
XI	187	1.25	1	2	0.71	0.58	0.14	96

The set VIII reproduces the pion decay constant

$$m_q = 255\,\text{MeV},\ m_g = 637.5\,\text{MeV and } \Lambda = 306\,\text{MeV}$$

Quantitative results: Static properties

WP, Ydrefors, Nogueira, Frederico and Salme PRD 103 014002 (2021).

Set	m (MeV)	B/m	μ/m	Λ/m	P_{val}	$P_{\uparrow\downarrow}$	$P_{\uparrow\uparrow}$	f_π (MeV)
I	187	1.25	0.15	2	0.64	0.55	0.09	77
II	255	1.45	1.5	1	0.65	0.55	0.10	112
III	255	1.45	2	1	0.66	0.56	0.11	117
IV	215	1.35	2	1	0.67	0.57	0.11	98
V	187	1.25	2	1	0.67	0.56	0.11	84
VI	255	1.45	2.5	1	0.68	0.56	0.11	122
VII	255	1.45	2.5	1.1	0.69	0.56	0.12	127
VIII	255	1.45	2.5	1.2	0.70	0.57	0.13	130
IX	255	1.45	1	2	0.70	0.57	0.14	134
X	215	1.35	1	2	0.71	0.57	0.14	112
XI	187	1.25	1	2	0.71	0.58	0.14	96

The set VIII reproduces the pion decay constant

$$m_q = 255\,\text{MeV},\, m_g = 637.5\,\text{MeV and } \Lambda = 306\,\text{MeV}$$

The contributions beyond the valence component are important, $\sim 30\%$

Quantitative results: Static properties

WP, Ydrefors, Nogueira, Frederico and Salme PRD 103 014002 (2021).

Set	m (MeV)	B/m	μ/m	Λ/m	P_{val}	$P_{\uparrow\downarrow}$	$P_{\uparrow\uparrow}$	f_π (MeV)
I	187	1.25	0.15	2	0.64	0.55	0.09	77
II	255	1.45	1.5	1	0.65	0.55	0.10	112
III	255	1.45	2	1	0.66	0.56	0.11	117
IV	215	1.35	2	1	0.67	0.57	0.11	98
V	187	1.25	2	1	0.67	0.56	0.11	84
VI	255	1.45	2.5	1	0.68	0.56	0.11	122
VII	255	1.45	2.5	1.1	0.69	0.56	0.12	127
VIII	255	1.45	2.5	1.2	0.70	0.57	0.13	130
IX	255	1.45	1	2	0.70	0.57	0.14	134
X	215	1.35	1	2	0.71	0.57	0.14	112
XI	187	1.25	1	2	0.71	0.58	0.14	96

The set VIII reproduces the pion decay constant

$$m_q = 255\,\text{MeV},\, m_g = 637.5\,\text{MeV and } \Lambda = 306\,\text{MeV}$$

The contributions beyond the valence component are important, $\sim 30\%$

The Valence probability has a small variation for the range of parameters

Parton distribution function

WP, Ydrefors, Nogueira, Frederico and Salme PRD 103 014002 (2021).

Parton distribution function

WP, Ydrefors, Nogueira, Frederico and Salme PRD 103 014002 (2021).

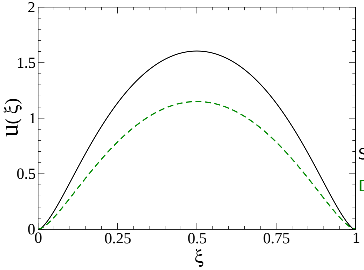

Solid line: full calculation of the BSE at model scale

Dashed line: The LF valence contribution

Parton distribution function

WP, Ydrefors, Nogueira, Frederico and Salme PRD 103 014002 (2021).

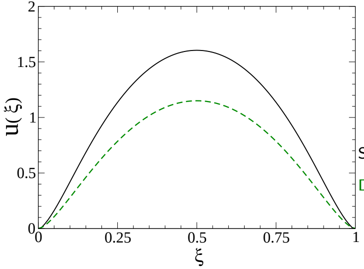

Solid line: full calculation of the BSE at model scale

Dashed line: The LF valence contribution

The symmetry of the PDFs is related to the charge symmetry.

Parton distribution function

WP, Ydrefors, Nogueira, Frederico and Salme PRD 103 014002 (2021).

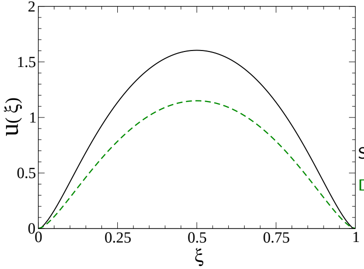

Solid line: full calculation of the BSE at model scale

Dashed line: The LF valence contribution

The symmetry of the PDFs is related to the charge symmetry.

The full PDF is normalized to 1, while the Valence PDF has norm 0.7

Parton distribution function

WP, Ydrefors, Nogueira, Frederico and Salme PRD 103 014002 (2021).

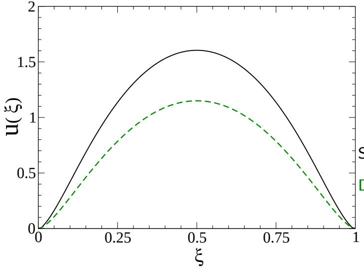

Solid line: full calculation of the BSE at model scale

Dashed line: The LF valence contribution

The symmetry of the PDFs is related to the charge symmetry.

The full PDF is normalized to 1, while the Valence PDF has norm 0.7

The difference of 30% is due to the presence of higher Fock components.

Parton distribution function

WP, Ydrefors, Nogueira, Frederico and Salme PRD 103 014002 (2021).

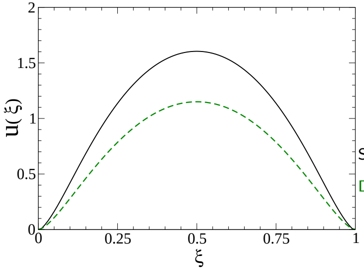

Solid line: full calculation of the BSE at model scale

Dashed line: The LF valence contribution

The symmetry of the PDFs is related to the charge symmetry.

The full PDF is normalized to 1, while the Valence PDF has norm 0.7

The difference of 30% is due to the presence of higher Fock components.

At the initial scale, for $\xi \to 1$, the exponent of $(1-\xi)^{\eta_0}$ is $\eta_0 = 1.4$

Parton distribution function

WP, Ydrefors, Nogueira, Frederico and Salme PRD 105 L071505 (2022).

Parton distribution function

WP, Ydrefors, Nogueira, Frederico and Salme PRD 105 L071505 (2022).

Low order Mellin moments at scales $Q = 2.0$ GeV and $Q = 5.2$ GeV.

	BSE_2	$LQCD_2$	BSE_5	$LQCD_5$
$\langle x \rangle$	0.259	0.261 ± 0.007	0.221	0.229 ± 0.008
$\langle x^2 \rangle$	0.105	0.110 ± 0.014	0.082	0.087 ± 0.009
$\langle x^3 \rangle$	0.052	0.024 ± 0.018	0.039	0.042 ± 0.010
$\langle x^4 \rangle$	0.029		0.021	0.023 ± 0.009
$\langle x^5 \rangle$	0.018		0.012	0.014 ± 0.007
$\langle x^6 \rangle$	0.012		0.008	0.009 ± 0.005

LQCD, $Q = 2.0$ GeV: $\langle x \rangle$ - Alexandrou et al PRD 103, 014508 (2021)

$\langle x^2 \rangle$ and $\langle x^3 \rangle$ - Alexandrou et al PRD 104, 054504 (2021)

LQCD, $Q = 5.0$ GeV: $\langle x \rangle$ - Alexandrou et al PRD 103, 014508 (2021)

Parton distribution function

WP, Ydrefors, Nogueira, Frederico and Salme PRD 105 L071505 (2022).

Low order Mellin moments at scales $Q = 2.0$ GeV and $Q = 5.2$ GeV.

	BSE_2	LQCD_2	BSE_5	LQCD_5
$\langle x \rangle$	0.259	0.261 ± 0.007	0.221	0.229 ± 0.008
$\langle x^2 \rangle$	0.105	0.110 ± 0.014	0.082	0.087 ± 0.009
$\langle x^3 \rangle$	0.052	0.024 ± 0.018	0.039	0.042 ± 0.010
$\langle x^4 \rangle$	0.029		0.021	0.023 ± 0.009
$\langle x^5 \rangle$	0.018		0.012	0.014 ± 0.007
$\langle x^6 \rangle$	0.012		0.008	0.009 ± 0.005

LQCD, $Q = 2.0$ GeV: $\langle x \rangle$ - Alexandrou et al PRD 103, 014508 (2021)

$\langle x^2 \rangle$ and $\langle x^3 \rangle$ - Alexandrou et al PRD 104, 054504 (2021)

LQCD, $Q = 5.0$ GeV: $\langle x \rangle$ - Alexandrou et al PRD 103, 014508 (2021)

Hadronic scale and effective charge for DGLAP

$Q_0 = 0.330 \pm 0.030$ GeV - Cui et al EPJC 2020 80 1064

Parton distribution function

WP, Ydrefors, Nogueira, Frederico and Salme PRD 105 L071505 (2022).

Low order Mellin moments at scales $Q = 2.0$ GeV and $Q = 5.2$ GeV.

	BSE_2	LQCD_2	BSE_5	LQCD_5
$\langle x \rangle$	0.259	0.261 ± 0.007	0.221	0.229 ± 0.008
$\langle x^2 \rangle$	0.105	0.110 ± 0.014	0.082	0.087 ± 0.009
$\langle x^3 \rangle$	0.052	0.024 ± 0.018	0.039	0.042 ± 0.010
$\langle x^4 \rangle$	0.029		0.021	0.023 ± 0.009
$\langle x^5 \rangle$	0.018		0.012	0.014 ± 0.007
$\langle x^6 \rangle$	0.012		0.008	0.009 ± 0.005

LQCD, $Q = 2.0$ GeV: $\langle x \rangle$ - Alexandrou et al PRD 103, 014508 (2021)

$\langle x^2 \rangle$ and $\langle x^3 \rangle$ - Alexandrou et al PRD 104, 054504 (2021)

LQCD, $Q = 5.0$ GeV: $\langle x \rangle$ - Alexandrou et al PRD 103, 014508 (2021)

Hadronic scale and effective charge for DGLAP

$Q_0 = 0.330 \pm 0.030$ GeV - Cui et al EPJC 2020 80 1064

Within the error, we choose $Q_0 = 0.360$ GeV to fit the first Mellin moment.

We used lowest order DGLAP equations for evolution

Parton distribution function

WP, Ydrefors, Nogueira, Frederico and Salm PRD 105, L071505 (2022).

Parton distribution function

WP, Ydrefors, Nogueira, Frederico and Salm PRD 105, L071505 (2022).

Comparison with experimental data

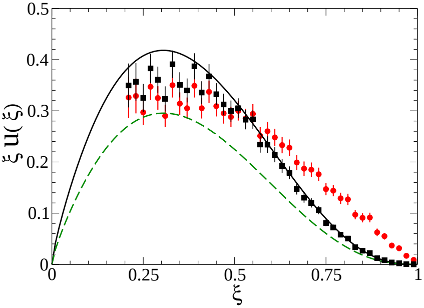

Solid line: full calculation of the BSE evolved from the initial scale $Q_0 = 0.360$ GeV to $Q = 5.2$ GeV

Dashed line: The evolved LF valence contribution

Full dots: experimental data from E615

Full squares: reanalyzed experimental data from Aicher et al PRL 105, 252003 (2010). evolved to $Q = 5.2$ GeV

Parton distribution function

WP, Ydrefors, Nogueira, Frederico and Salm PRD 105, L071505 (2022).

Parton distribution function

WP, Ydrefors, Nogueira, Frederico and Salm PRD 105, L071505 (2022).

Comparison with other theoretical calculations

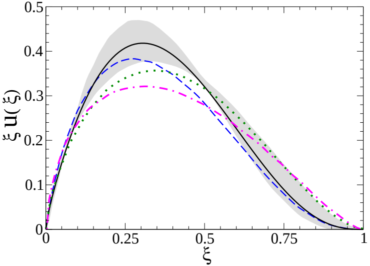

Solid line: full calculation of the BSE evolved

from the initial scale $Q_0 = 0.360$ GeV to $Q = 5.2$ GeV

Dashed line: DSE calculation (Cui et al)

Dash-dotted line: DSE calculation with dressed quark-photon vertex

from Bednar et al PRL 124, 042002 (2020)

Dotted line: BLFQ colaboration, PLB 825, 136890 (2022)

Gray area: LQCD results from C. Alexandrou et al (2021)

It is in agreement with PQCD, exponent greater than 2

Parton distribution function

WP, Ydrefors, Nogueira, Frederico and Salm PRD 105, L071505 (2022).

Comparison with other theoretical calculations

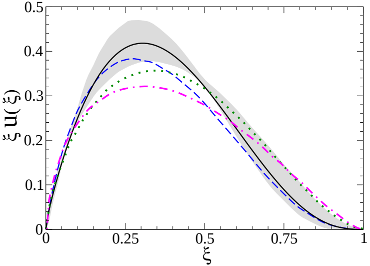

Solid line: full calculation of the BSE evolved

from the initial scale $Q_0 = 0.360$ GeV to $Q = 5.2$ GeV

Dashed line: DSE calculation (Cui et al)

Dash-dotted line: DSE calculation with dressed quark-photon vertex

from Bednar et al PRL 124, 042002 (2020)

Dotted line: BLFQ colaboration, PLB 825, 136890 (2022)

Gray area: LQCD results from C. Alexandrou et al (2021)

It is in agreement with PQCD, exponent greater than 2

Evolved $\xi\, u(\xi)$, for $\xi \to 1$, the exponent of $(1-\xi)^{\eta_5}$ is $\eta_5 = 2.94$

LQCD: Alexandrou et al PRD 104, 054504 (2021) obtained 2.20 ± 0.64

Cuit et al EPJA 58, 10 (2022) obtained 2.81 ± 0.08

Pion image on the null-plane

The probability distribution of the quarks inside the pion, on the light-front, is evaluated in the space given by the Cartesian product of the Ioffe-time and the plane spanned by the transverse coordinates.

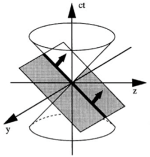

Pion image on the null-plane

The probability distribution of the quarks inside the pion, on the light-front, is evaluated in the space given by the Cartesian product of the Ioffe-time and the plane spanned by the transverse coordinates.

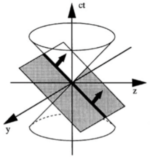

Our goal is to use the configuration space in order to have a more detailed information of the space-time structure of the hadrons.

Pion image on the null-plane

The probability distribution of the quarks inside the pion, on the light-front, is evaluated in the space given by the Cartesian product of the Ioffe-time and the plane spanned by the transverse coordinates.

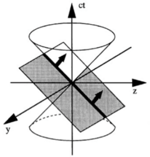

Our goal is to use the configuration space in order to have a more detailed information of the space-time structure of the hadrons.

The Ioffe-time (Miller and Brodsky) is useful for studying the relative importance of short and long light-like distances. It is defined as:

$$\tilde{z} = x \cdot P_{target} = x^{-}\, P^{+}_{target}/2 \text{ on the hyperpane } x^{+} = 0.$$

Pion image on the null-plane

We perform a Fourier transform of the valence wf

The space-time structure of the pion in terms of Ioffe-time $\tilde{z} = x^- \, p^+/2$ and the transverse coordinates $\{b_x, b_y\}$

The pion $b_\perp |\psi|^2$ in the 3D Ioffe-space

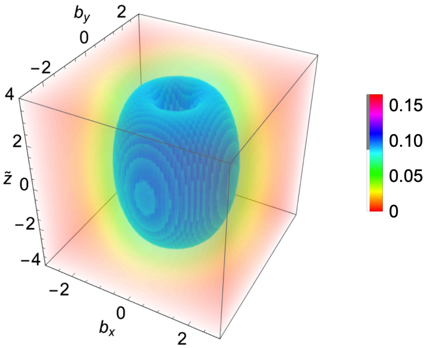

Pion charge radius

Ydrefors, WP, Nogueira, Frederico and Salmè PLB 820, 136494 (2021)

Pion charge radius

Ydrefors, WP, Nogueira, Frederico and Salmè PLB 820, 136494 (2021)

Pion charge radius and its decomposition in valence and non valence contributions.

Set	m	B/m	μ/m	Λ/m	P_{val}	f_π	r_π (fm)	r_{val} (fm)	r_{nval} (fm)
I	255	1.45	2.5	1.2	0.70	130	0.663	0.710	0.538
II	215	1.35	2	1	0.67	98	0.835	0.895	0.703

where $r_\pi^2 = -6\ dF_\pi(Q^2)/dQ^2\Big|_{Q^2=0}$

$$P_{\rm val(nval)}\ r^2_{\rm val(nval)} = -6\ dF_{\rm val(nval)}(Q^2)/dQ^2\Big|_{Q^2=0}$$

Pion charge radius

Ydrefors, WP, Nogueira, Frederico and Salmè PLB 820, 136494 (2021)

Pion charge radius and its decomposition in valence and non valence contributions.

Set	m	B/m	μ/m	Λ/m	P_{val}	f_π	r_π (fm)	r_{val} (fm)	r_{nval} (fm)
I	255	1.45	2.5	1.2	0.70	130	0.663	0.710	0.538
II	215	1.35	2	1	0.67	98	0.835	0.895	0.703

where $r_\pi^2 = -6\ dF_\pi(Q^2)/dQ^2\Big|_{Q^2=0}$

$$P_{\mathrm{val(nval)}}\ r^2_{\mathrm{val(nval)}} = -6\ dF_{\mathrm{val(nval)}}(Q^2)/dQ^2\Big|_{Q^2=0}$$

The set I is in fair agreement with the PDG value:

$$r_\pi^{PDG} = 0.659 \pm 0.004 \text{ fm}$$

Electromagnetic Form Factor

Ydrefors, WP, Nogueira, Frederico and Salmè PLB 820, 136494 (2021)

Electromagnetic Form Factor

Ydrefors, WP, Nogueira, Frederico and Salmè PLB 820, 136494 (2021)

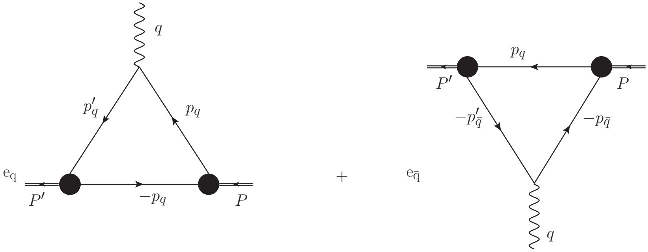

Electromagnetic Form Factor

Ydrefors, WP, Nogueira, Frederico and Salmè PLB 820, 136494 (2021)

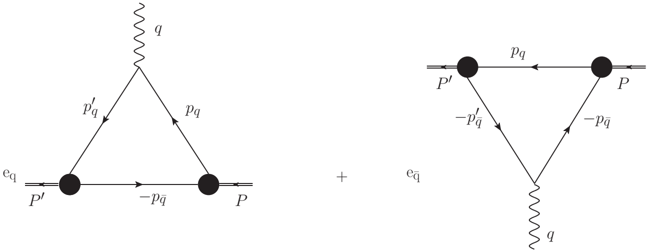

The elastic FF is given by

$$F(Q^2) = -i\ \frac{N_c}{M^2\ (1+\tau)} \int \frac{d^4 p_{\bar{q}}}{(2\pi)^4}\ \mathrm{Tr}\left[(-\not{p}_{\bar{q}} - m)\bar{\Phi}(k';P')(\not{P} + \not{P}')\ \Phi(k;P)\right]$$

Electromagnetic Form Factor

Ydrefors, WP, Nogueira, Frederico and Salmè PLB 820, 136494 (2021)

Electromagnetic Form Factor

Ydrefors, WP, Nogueira, Frederico and Salmè PLB 820, 136494 (2021)

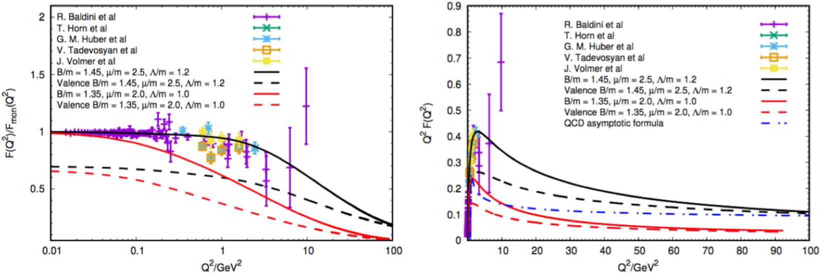

$$m_q = 255\text{MeV}, m_g = 637\text{MeV and } \Lambda = 306\text{MeV}$$

Electromagnetic Form Factor

Ydrefors, WP, Nogueira, Frederico and Salmè PLB 820, 136494 (2021)

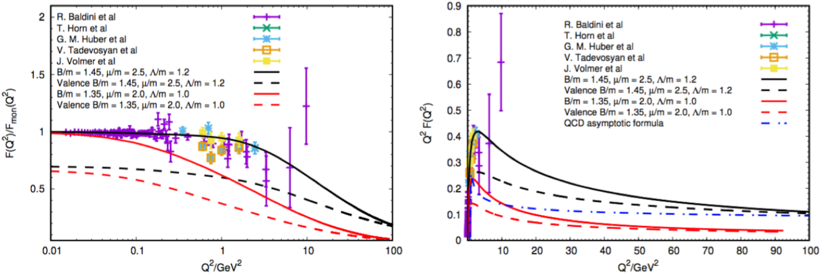

$$m_q = 255\text{MeV}, m_g = 637\text{MeV and } \Lambda = 306\text{MeV}$$

Good agreement with experimental data (black curve).
For high Q^2 we obtain the valence dominance (dashed black curve)
Our results recover the pQCD for large Q^2 - Blue curve vs Black curve

Transverse Momentum Distributions

Unpolarized transverse-momentum dependent quark distributions

Transverse Momentum Distributions

Unpolarized transverse-momentum dependent quark distributions

TMD's are important for parametrizing the hadronic quark-quark correlator

Transverse Momentum Distributions

Unpolarized transverse-momentum dependent quark distributions

TMD's are important for parametrizing the hadronic quark-quark correlator

One can define the T-even subleading quark uTMDs, starting from the decomposition of the pion correlator (Mulders and Tangerman, Nucl. Phys. B 461, 197 (1996)).

Transverse Momentum Distributions

Unpolarized transverse-momentum dependent quark distributions

TMD's are important for parametrizing the hadronic quark-quark correlator

One can define the T-even subleading quark uTMDs, starting from the decomposition of the pion correlator (Mulders and Tangerman, Nucl. Phys. B 461, 197 (1996)).

twist-3 uTMD (See Lorcé, Pasquini, and Schweitzer, EPJC 76, 415 (2016)):

$$\frac{M}{P^+}\, e^q(\gamma,\xi) = \frac{N_c}{4}\int d\phi_{\hat{\mathbf{k}}_\perp}\int_{-\infty}^{\infty}\frac{dy^-\, d\mathbf{y}_\perp}{2(2\pi)^3}\, e^{i[\xi P^+ y^-/2-\mathbf{k}_\perp\cdot\mathbf{y}_\perp]}\,\langle P|\bar{\psi}_q(-\frac{y}{2})\,\hat{1}\,\psi_q(\frac{y}{2})|P\rangle\big|_{y^+=0}$$

$$\frac{M}{P^+}\, f^{\perp q}(\gamma,\xi) = \frac{N_c M}{4\gamma}\int d\phi_{\hat{\mathbf{k}}_\perp}\int_{-\infty}^{\infty}\frac{dy^-\, d\mathbf{y}_\perp}{2(2\pi)^3}\, e^{i[\xi P^+ y^-/2-\mathbf{k}_\perp\cdot\mathbf{y}_\perp]}\,\langle P|\bar{\psi}_q(-\frac{y}{2})\,\mathbf{k}_\perp\cdot\boldsymbol{\gamma}_\perp\,\psi_q(\frac{y}{2})|P\rangle\big|_{y^+=0}$$

Transverse Momentum Distributions

Unpolarized transverse-momentum dependent quark distributions

TMD's are important for parametrizing the hadronic quark-quark correlator

One can define the T-even subleading quark uTMDs, starting from the decomposition of the pion correlator (Mulders and Tangerman, Nucl. Phys. B 461, 197 (1996)).

twist-3 uTMD (See Lorcé, Pasquini, and Schweitzer, EPJC 76, 415 (2016)):

$$\frac{M}{P^+}\ e^q(\gamma,\xi) = \frac{N_c}{4}\int d\phi_{\hat{\mathbf{k}}_\perp}\int_{-\infty}^{\infty}\frac{dy^-\,d\mathbf{y}_\perp}{2(2\pi)^3}\ e^{i[\xi P^+ y^-/2-\mathbf{k}_\perp\cdot\mathbf{y}_\perp]}\ \langle P|\bar{\psi}_q(-\frac{y}{2})\ \hat{1}\ \psi_q(\frac{y}{2})|P\rangle\big|_{y^+=0}$$

$$\frac{M}{P^+}\ f^{\perp q}(\gamma,\xi) = \frac{N_c M}{4\gamma}\int d\phi_{\hat{\mathbf{k}}_\perp}\int_{-\infty}^{\infty}\frac{dy^-\,d\mathbf{y}_\perp}{2(2\pi)^3}\ e^{i[\xi P^+ y^-/2-\mathbf{k}_\perp\cdot\mathbf{y}_\perp]}\ \langle P|\bar{\psi}_q(-\frac{y}{2})\ \mathbf{k}_\perp\cdot\boldsymbol{\gamma}_\perp\ \psi_q(\frac{y}{2})|P\rangle\big|_{y^+=0}$$

twist-4 uTMD

$$\left(\frac{M}{P^+}\right)^2\ f_4^q(\gamma,\xi) = \frac{N_c}{4}\int d\phi_{\hat{\mathbf{k}}_\perp}\int_{-\infty}^{\infty}\frac{dy^-\,d\mathbf{y}_\perp}{2(2\pi)^3}\ e^{i[\xi P^+ y^-/2-\mathbf{k}_\perp\cdot\mathbf{y}_\perp]}\ \langle P|\bar{\psi}_q(-\frac{y}{2})\ \gamma^-\ \psi_q(\frac{y}{2})|P\rangle\big|_{y^+=0}$$

Transverse Momentum Distributions

Transverse Momentum Distributions

twist-3 uTMD

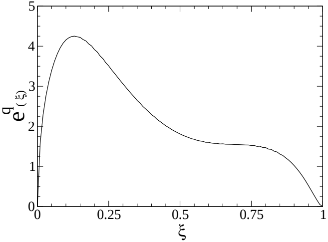

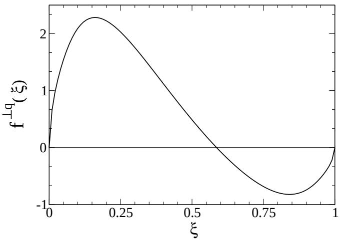

Transverse Momentum Distributions

twist-3 uTMD

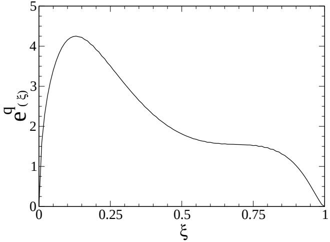

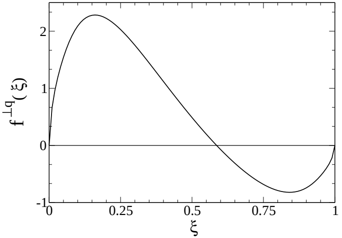

twist-4 uTMD

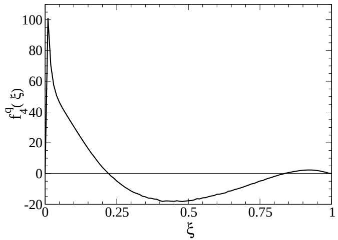

Conclusions and Perspectives

- We present a method for solving the fermionic BSE in Minkowski space.
- We obtain the PDF, charge radius and Electromagnetic Form Factor.
- Furthermore, the image of the pion in the configuration space has been constructed. This 3D imaging is in line with the goal of the future Electron Ion Collider.
- We present first results for the uTMD. We intend to complete this analysis and calculate GPDs.
- Future plan is to include dressing functions for quark and gluon propagators and a more realistic quark-gluon vertex (Dyana's talk).